
Article:
Trickey, William, Walsh, Jamie and Pasley, John Richard (2022) Time-dependent subsonic ablation pressure scalings for soft X-ray heated low- and intermediate-Z materials at drive temperatures of up to 400 eV. HIGH ENERGY DENSITY PHYSICS. 100995. ISSN: 1574-1818

High Energy Density Physics 44 (2022) 100995

Contents lists available at ScienceDirect

High Energy Density Physics

journal homepage: www.elsevier.com/locate/hedp

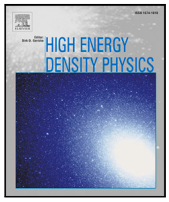

Time-dependent subsonic ablation pressure scalings for soft X-ray heated low- and intermediate-Z materials at drive temperatures of up to 400 eV

William Trickey, Jamie Walsh, John Pasley *

York Plasma Institute, Department of Physics, University of York, Heslington, York, YO10 5DD, UK

ARTICLE INFO

Keywords:
X-ray ablation
Indirect drive ICF
Radiation-hydrodynamics

ABSTRACT

The soft X-ray driven subsonic ablation of five different materials with atomic numbers ranging from 3.5 to 22 is investigated for radiation drive temperatures of up to 400 eV. Simulations were performed using the one-dimensional radiation hydrodynamics simulation code HYADES. For each material, ablation pressure scaling-laws are determined as a function of drive radiation-temperature and time, assuming that the irradiation lasts for a period of a few nanoseconds and that the drive temperature remains constant during this period. For all the materials, the maximum drive-temperature for subsonic operation is identified. As expected, lower-Z materials demonstrate a stronger scaling of ablation pressure with radiation temperature and a more gradual fall off with time. However, the lowest-Z materials transition to trans- and super-sonic ablation at temperatures of only a few hundred eV.

1. Introduction

The interaction of intense, soft X-ray radiation with matter is of substantial interest in the field of high energy–density physics, and is thought to be responsible for a number of important astrophysical phenomena, perhaps even triggering the gravitational collapse of gas clouds leading to stellar formation. Other examples can be found in the dynamics of gaseous nebulae and in the formation of ionisation waves as the intense radiation field from a newly formed star interacts with its surroundings. In the past few decades there has been considerable interest in the generation of intense, soft X-ray radiation in the laboratory and the possibility of using this radiation as a driver for inertial confinement fusion (ICF). In this application, driver energy, typically in the form of laser photons, is converted to soft X-rays by irradiating the interior of a high atomic-number (high-Z) hohlraum, causing it to radiate thermally with a radiation temperature of up to a few hundred eV. These X-rays in turn irradiate a low atomic-number (low-Z) spherical target, causing it to implode violently with the intention of creating the conditions necessary for thermonuclear fusion as the material stagnates centrally.

When an intense soft X-ray radiation field is incident upon a cold low-Z target at solid density, the X-rays will initially penetrate in to a depth of approximately one radiation mean free path. Due to the intensity of the drive, this surface material is simultaneously heated and ionised. This causes the opacity of the surface material to the incident radiation to be reduced, allowing the radiation from the source to penetrate into the as-yet unheated target material. With a high-Z target the mechanism differs somewhat in that the opacity of the heated material to the incident photons remains significantly higher than in the case of a lower-Z material. This rapidly gives rise to diffusive (Marshak wave [1]) heating. In either case, the region in which the material transitions from being cold and unionised to hot and ionised is known as an ionisation front. X-ray heating of matter also exhibits an interesting range of phenomenology depending on the intensity and spectral temperature of the incident X-ray flux and the material properties of the target. Sub-, trans- and super-sonic ionisation waves may be formed, where the terminology used references the speed of propagation of the ionisation front relative to the speed of sound in the hot material.

Subsonic propagation, in which the heat front propagates into the material at less than the speed of sound in the heated material, gives rise to significant gross hydrodynamic behaviour and the formation of a radiatively supported shock wave. The result is a momentum-conserving ablation wave in which hot material is ejected back toward the drive to balance the forward momentum of the shocked material. In the extreme of supersonic behaviour, by comparison, the heating is so rapid that negligible forward going hydrodynamic motion results.

In the present study we are chiefly interested in producing results that are of interest for the ablative acceleration of homogeneous solid targets by the direct application of soft X-rays. Whilst there are ways to utilise supersonic heat waves in payload acceleration, these require

* Corresponding author.
E-mail address: john.pasley@york.ac.uk (J. Pasley).

https://doi.org/10.1016/j.hedp.2022.100995
Received 1 March 2022; Received in revised form 23 June 2022; Accepted 2 August 2022
Available online 10 August 2022

more involved set-ups [2] since, as noted, supersonic heating is less effective in producing forward motion in the irradiated sample. Transonic behaviour, in which the heat wave and shock wave tend to over-lap, and the heat front propagates at approximately the sound speed in the hot matter, is mainly considered here as the point at which such subsonic ablative acceleration ceases to be effectual.

Substantial work has already been performed on this topic, much of it in connection to ICF, which relies upon subsonic heating to drive the implosion of the fuel capsule. However, this focus upon ICF has inevitably meant that the majority of non-astrophysical studies of X-ray driven ablative behaviour have concentrated upon ICF-capsule relevant materials. The astrophysical literature has conversely tended to focus upon astro-relevant materials (hydrogen!). These studies do not provide ready answers to questions about the acceleration of payloads with soft X-ray driven subsonic ablation in general. The existing ICF related literature on the topic has tended to focus upon CH-plastics, beryllium and high-density carbon, as these are the materials commonly used in ICF capsule ablators [3–7] and only at temperatures up to around 350 eV. Studies related to hohlraum wall materials, such as gold and uranium, have naturally tended to focus more upon their radiative properties rather than the pressures produced at the wall, since this has little import for the ICF target designer. This study aims to address this in a limited way, by providing some simple scalings that may be used to provide estimates for the time-dependent ablation pressures achievable with a range of low- and intermediate-Z materials, with atomic number up to 22, for soft X-ray drive temperatures of up to 400 eV. Higher-Z elements necessarily require a more sophisticated treatment of the atomic physics than that which is employed here, and may exhibit a more complicated relationship between radiation temperature and ablation pressure than is exhibited by the materials considered here.

A potential benefit of low-Z ablators for ICF applications is made apparent by the ideal rocket equation [8]:

$$V_{shell} = \frac{P_a}{\dot{m}} ln\left(\frac{m_0}{m_f}\right) \equiv V_{exhaust}\, ln\left(\frac{m_0}{m_f}\right) \tag{1}$$

where m_0 is the initial shell mass, m_f is the final shell mass, P_a is the ablation pressure, $\dot{m}$ is the mass ablation rate per unit area and V is the velocity of the shell or the exhaust material (as identified by the subscript). ICF capsule implosions are designed to exceed a threshold implosion velocity in order to couple enough energy to the fuel to trigger ignition [9–11]. From Eq. (1) it can be seen that an increase in the velocity of the ablated material results in an increased implosion velocity. The lower the ion mass, the higher the velocity of the ion upon ablation at a given temperature. Therefore, low-Z ablators are more efficient at accelerating the shell. This model clearly demonstrates one of the potential benefits of a low-Z ablator but it does not account for other parameters that affect radiation coupling, such as albedo. Such effects can be particularly important in the case of high-Z ablators and/or where the drive pulse is relatively long. In such cases the opacity of the material lying between the X-ray source and the cold ablator becomes an increasingly significant factor in determining the achievable pressures.

2. Analytical pressure scaling

The scaling of ablation pressure with radiation drive temperature is dependent on the regime of energy deposition and plasma flow. Three possible regimes exist: subsonic, transonic and supersonic. In the subsonic case, a shock wave propagates ahead of the X-ray driven heat front, compressing the material ahead of it, and coupling forward momentum to this compressed fluid, which balances the momentum flow back toward the drive. The scaling of ablation pressure with drive temperature is strong in the subsonic case; dimensional analysis, whereby irradiance is balanced by the outflow of heated material, suggests a scaling of ablation pressure with the drive radiation temperature of $P_a \propto T_R^{3.5}$. (Note that in what follows it is assumed that the drive intensity and spectral characteristics are both well described by a single radiation temperature.) In the limit of extreme supersonic behaviour, however, no shock front is formed and the heat front propagates so rapidly through the material that it does not respond hydrodynamically. One may consider that the heat wave is propagating through the fluid at such a speed that the associated pressure gradient acts on a given region of fluid for so short a period of time that the net acceleration is negligible. The case of supersonic radiative heating is sometimes referred to as *volume heating* which, in its extreme limit, propagates through the material at the speed of light [12–14]. In the case of highly supersonic heating, the pressure generated at the heat front is simply given by nkT, though ionisation may mean that this is a stronger than linear scaling with temperature. In the transonic regime the scaling becomes non-trivial and may exhibit hysteresis depending upon whether one is approaching it from the sub- or supersonic regime. This hysteresis effect is due to the fact that if the drive temperature is increasing from the subsonic regime then the drive must penetrate through the compressed region lying between it and the cold fluid, which retards its progress.

For a low-Z material, due to the low opacity of the ablative blow-off stationary ablation can be assumed. Stationary ablation is the situation in which a transparent, low density isothermal ablative blow-off region is separated from a compressed region via a discontinuous boundary called the ablation front. This system can be modelled using Rankine–Hugoniot relations in a similar manner to shock fronts. If the blow-off region is denoted with subscript 1 and the compressed region 0, the relations are

$$\rho_1 u_1 = \rho_0 u_0, \tag{2}$$

$$\rho_1 u_1^2 + P_1 = \rho_0 u_0^2 + P_0, \tag{3}$$

$$e_1 + \frac{u_1^2}{2} + \frac{P_1}{\rho_1} = e_1 + \frac{u_0^2}{2} + \frac{P_0}{\rho_0} + \Delta e, \tag{4}$$

where ρ is mass density, u is fluid velocity, p is pressure and e is specific energy. Δe is the specific energy deposited at the ablation front by the incoming X-ray radiation. The energy from the X-ray flux will either be deposited in the compressed material or into the ablative blow-off in order to keep it isothermal. Including a term required to keep the blow-off region isothermal, the flux balance is

$$\sigma T_R^4 = \rho_1 v_1 \Delta e + \rho_1 c_T^3, \tag{5}$$

where σ is the Stefan–Boltzmann constant, T_R is the radiation temperature of the X-ray drive and c_T is the isothermal sound speed. The transition from the subsonic to the supersonic regime will occur when the fluid velocity in the blow-off region exceeds the isothermal sound speed $v_1 > c_T$. If this condition is substituted into the jump conditions (2)–(4) and the flux balance equation, using $c_T = (T_R R/\mu)^{1/2}$ we can express a critical drive temperature at which this transition will occur:

$$T_{R,\text{critical}} \approx \left(\frac{4\rho}{\sigma}\right)^{\frac{2}{5}} \left(\frac{\mathrm{R}}{\mu}\right)^{\frac{3}{5}} \tag{6}$$

where R is the gas constant and μ is the fully ionised molecular weight, given by:

$$\mu = \frac{A}{Z+1}, \tag{7}$$

where Z and A are respectively the atomic number and mass number of one average-atom of the material. Eq. (6) simplifies to:

$$T_{R,\text{critical}}(100\text{ eV}) \approx 4.23 \rho^{\frac{2}{5}} \mu^{-\frac{3}{5}}. \tag{8}$$

with the density in units of g/cm^3. A full treatment of the derivation of Eq. (6) can be found in Ref. [15]. For temperatures sufficiently below $T_{R,\text{critical}}$ Eq. (4) is well approximated by the relation [16]

$$P_0 = \frac{\sigma T_R^4}{\sqrt{4 T_R R/\mu}}. \tag{9}$$

This is the origin of the $P_a \propto T_R^{3.5}$ scaling discussed earlier. For temperatures above $T_{R,\text{critical}}$ the scaling of ablation pressure with drive temperature is expected to weaken. The formalism by which this scaling of $T_{R,\text{critical}}$ is derived means that it is expected to hold less well once the Z is sufficiently high that the opacity of the heated material becomes significant, and, for similar reasons, it may cease to hold well even for relatively low-Z materials in the case that the heat front propagates deeply into the material.

3. Radiation hydrodynamics simulations

The results presented in this section are produced using the code HYADES, a one-dimensional (1-D) Lagrangian hydrodynamics and energy transport code [17]. In total three hundred and ten simulations were performed to produce the results shown in this study. In each simulation a 1 mm thick slab of material at an initial temperature of 300 K is irradiated with a Planckian X-ray source. The radiation flux rises linearly from zero to the intended value of T_R in 10 ps, remaining constant thereafter. For all materials other than titanium, EOS was handled with SESAME look-up tables; the titanium simulations used a quotidian equation of state [18]. The radiation transport was handled with a multi-group diffusion model. The multi-group optical absorption coefficients employed in these simulations are generated in-line by the Atomic Physics and Opacity Package (APOP) of HYADES. These opacities are functions of the material composition, density and temperature, which determine the populations and energies of the bound electrons as well as the free electrons of the continuum. A screened hydrogenic LTE model is employed, thus the ions and electrons in a given computational cell are characterised by a single kinetic temperature T for the purpose of the opacity calculations. This also permits the use of steady-state Boltzmann–Saha equations, which are functions only of the elemental composition, mass density, and temperature. Once the bound-level populations and their energies are determined, along with the free electron density, the frequency-dependent opacities can be found. For each prescribed frequency, there are free–free, bound–free, and bound–bound contributions. The bound–bound values are based on the Einstein coefficients for spontaneous emission (the A coefficients), absorption, and stimulated emission (the two B coefficients). The three Einstein coefficients are simply related to one another. It is then possible to calculate both the bound–bound emission and absorption coefficients. The bound–free quantities are based on the Einstein–Milne relations. Again, the spontaneous and stimulated probabilities are calculated, from which the emission and absorption coefficients are found; a quantum mechanical correction in the form of so-called Gaunt factors is included. The free–free quantities are determined by considering the radiation emitted by an electron moving in a Coulomb field; again, a separate Gaunt factor is required. The absorption coefficients are then used to solve the radiation transfer equation. Simulations are performed for each material at a range of radiation temperatures from 100 eV to 400 eV in steps of 10 eV.

Simulations are performed for five materials: CH-plastic, beryllium, carbon, aluminium, and titanium. The aluminium and titanium simulations were performed at 3/4 solid density in order bring the T_{crit} value below 400 eV, which is the maximum drive temperature explored in this study. In each case the simulations settle to give a relatively stable ablation pressure which then decays slowly over time. The results of these simulations can be seen for all materials in Fig. 1(a). The results for the CH-plastic and titanium are plotted separately in Figs. 1(b) and 1(c) as examples of the behaviour of low- and intermediate-Z materials respectively. In the plastic simulations the ablation pressure increases with drive temperature up to the critical temperature at which point transonic behaviour commences. Thereafter the ablation pressure decays somewhat with increasing temperature, before plateauing. If temperature is increased still further the pressure begins to rise up again, but in a more gradual fashion. This weaker scaling is typical of the supersonic regime. It can be seen in Fig. 1(b) that, for CH-plastic, the transition to transonic behaviour occurs at approximately 290 eV. We refer to the highest temperature simulated below this transition as the maximum drive temperature for the material. Any increase in temperature above this will result in a weaker pressure scaling. In the case of 3/4 solid density titanium it can be seen that, whilst the initial scaling is not as strong as for the low-Z plastic, the maximum drive temperature for titanium is higher at 340 eV, with much higher subsonic ablation pressures thereby being achievable with titanium provided that the temperature can be increased to close to this limiting value.

The approximate maximum drive temperature for the subsonic ablation of each of the materials investigated in this study is plotted in Fig. 2. The simulation results show significant deviation from the $T_{R,critical}$ values predicted by Eq. (8). This is due to the assumptions made about the equation of state. In the derivation of the analytical scaling law, an ideal gas equation of state was assumed whereas the simulations used more accurate models. The effects of the opacity model were also investigated. The absorption coefficient of radiation in HYADES can be modified manually. This absorption coefficient was multiplied by a value of 0.9–1.1. The results showed no variation in the $T_{R,critical}$ value suggesting it to be primarily a function of the equation of state of the material.

Due to the fact that the lowest-Z materials typically transition to transonic behaviour at temperatures below those required for laser-driven indirect drive ICF, such ICF capsules commonly include intermediate-Z dopant layers at depth in the ablator. Dopants are primarily used to prevent fuel preheat and increase the Atwood number of the shell [19] but an additional function is to shift the transition to transonic behaviour to a higher temperature, enabling the capsule to continue to operate as intended at the peak of the drive (~350 eV), for a short period, as required [20].

Further to determining the maximum drive temperature for subsonic ablation for the low- and mid-Z materials, an ablation pressure scaling is found in the subsonic regime for each of the materials investigated in this study. A scaling relationship of the form $P_a \propto T_R^{\alpha} t^{\beta}$ is found by applying non-linear regression fitting of the α and β parameters to the data independently. The data from which the T_R scaling results is obtained by recording the maximum pressure in each of a set of simulations performed over the range of 100 eV to the maximum drive temperature found for subsonic ablation. The t scaling is found by studying the temporal variation of the ablation pressure at a fixed radiation temperature of 250 eV. These time-scaling simulations were run for a total of 10 ns with the exception of plastic and beryllium which experienced shock breakouts at the rear surface of the 1 mm target at 6 ns and 8 ns respectively. The resultant scaling laws are shown in Table 1. As expected it is generally seen that the ablation pressure has a stronger temperature dependence and weaker time dependence for lower-Z materials. Unfortunately there exists little literature on the experimental measurement of time-dependent soft X-ray driven ablation pressures. Here we draw attention to the mass ablation rate studies in references [21,22] and [23] which suggest a scaling of $P_a \propto T_R^{3.5}$ for the low-Z materials, similar to those predicted here. Given that it is not possible to benchmark these scalings against experimental data at the present time, caution must be exercised in their application. Also it is worth re-iterating that the opacities here are based on a reduced model. Nevertheless, since comparable data has not been published elsewhere, it is hoped that these results will be of some use to the experimental community.

4. Conclusion

Soft X-ray driven ablation of materials, in the subsonic regime, is investigated with fixed radiation drive temperatures of up to 400 eV. 1-D radiation hydrodynamics simulations are used to study the ablation of five materials with atomic numbers ranging from 3.5 to 22. For all of the materials a maximum drive temperature for subsonic ablations is identified. Additionally, an ablation pressure scaling law suitable for

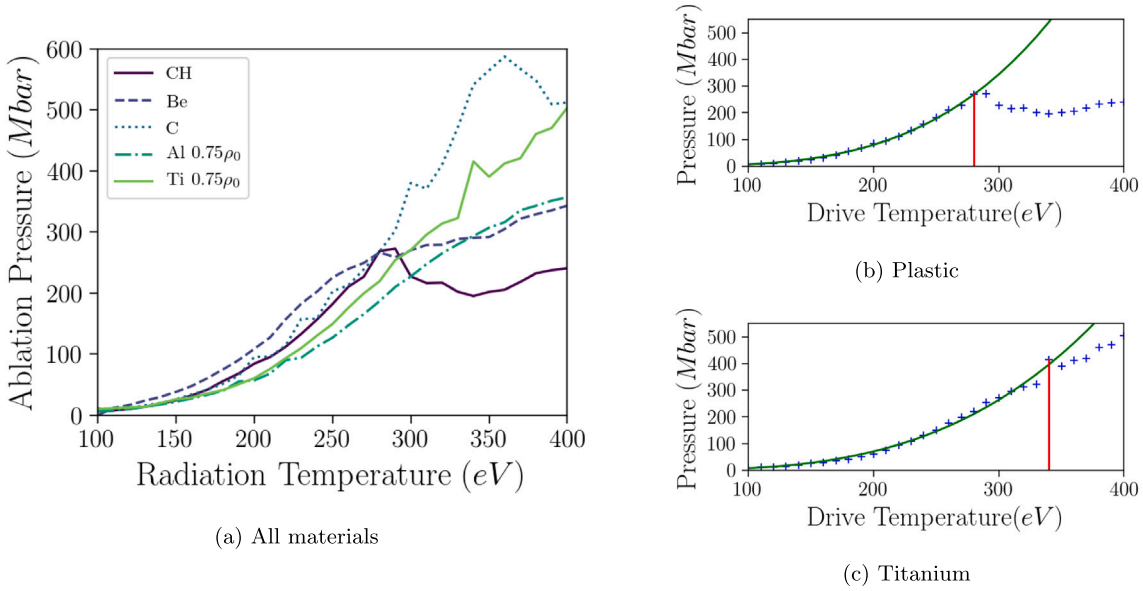

(a) All materials

(b) Plastic

(c) Titanium

Fig. 1. Plots of ablation pressure as a function of drive temperature for **(a)** all materials. The plots on the right show the results for **(b)** plastic and **(c)** titanium. Each cross represents the ablation pressure obtained from an individual simulation performed at a given drive temperature. A suggested maximum drive temperature is indicated by the vertical red line. In **(b)** and **(c)**, the fitted power laws from Table 1 are plotted as green lines.

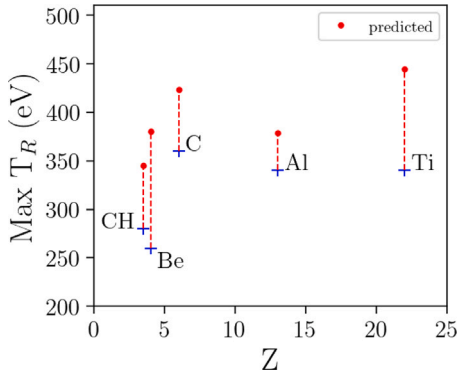

Fig. 2. Plots of the approximate maximum drive temperatures for subsonic ablation in the five materials as a function of atomic number, Z. The red dotted line shows the $T_{R,\text{critical}}$ value predicted by Eq. (8).

Table 1
Scaling laws for each material describing how ablation pressure changes with both drive temperature and time. The scaling for T_R and t is determined by finding the ablation pressure scaling with temperature and the simulations used to construct the temporal scaling are performed at a fixed drive temperature of 250 eV.

Material	Suggested scaling law	Max T_R
Plastic	$P_a \propto T_R^{3.6} t^{-0.07}$	280 eV
Beryllium	$P_a \propto T_R^{3.3} t^{-0.07}$	260 eV
Carbon	$P_a \propto T_R^{3.3} t^{-0.09}$	360 eV
Aluminium $0.75\rho_0$	$P_a \propto T_R^{3.2} t^{-0.17}$	340 eV
Titanium $0.75\rho_0$	$P_a \propto T_R^{3.2} t^{-0.21}$	340 eV

use in the subsonic regime is found as a function of drive radiation-temperature and time. Low-Z materials demonstrate a stronger scaling between ablation pressure and drive temperature and a weaker decay of ablation pressure with time. However, the lowest-Z ablators can only be used at relatively low temperatures since the ablation wave starts to propagate transonically at drive temperatures of a few hundred eV. In real experiments temperatures would likely not rise as rapidly as they do in these simulations, nor would they tend to be isothermal. However, the relatively weak temporal dependencies seen for the pressure in these low-Z and intermediate-Z materials indicates that the results of these simulations can still help to provide insight in situations where the temporal drive profile differs significantly from that modelled here, particularly as regards appropriate choice of ablator material.

Declaration of competing interest

The authors declare the following financial interests/personal relationships which may be considered as potential competing interests: W. Trickey reports financial support was provided by Engineering and Physical Sciences Research Council.

Data availability

Data will be made available on request.

Acknowledgements

The authors would like to thank R. Trines and R. Scott and the Rutherford Appleton Laboratory for providing access to and maintaining the computing systems on which HYADES is used. This work was supported by the Engineering and Physical Sciences Research Council, UK [EP/L01663X/1].

References

[1] R.E. Marshak, Phys. Fluids 1 (1958) 24.
[2] J. Pasley, P. Nilson, L. Willingale, M.G. Haines, M. Notley, M. Tolley, D. Neely, W. Nazarov, O. Willi, Phys. Plasmas 13 (2006) 032702.
[3] J. Lindl, O. Landen, J. Edwards, E. Moses, the NIC Team, Phys. Plasmas 21 (2014) 020501.
[4] S.W. Haan, J.D. Lindl, D.A. Callahan, D.S. Clark, J.D. Salmonson, B.A. Hammel, L.J. Atherton, R.C. Cook, M.J. Edwards, S. Glenzer, et al., Phys. Plasmas 18 (5) (2011) 051001.
[5] D.S. Clark, S.W. Haan, B.A. Hammel, J.D. Salmonson, D.A. Callahan, R.P.J. Town, Phys. Plasmas 17 (5) (2010) 052703.
[6] D.C. Wilson, P.A. Bradley, N.M. Hoffman, F.J. Swenson, D.P. Smitherman, R.E. Chrien, R.W. Margevicius, D.J. Thoma, L.R. Foreman, J.K. Hoffer, et al., Phys. Plasmas 5 (5) (1998) 1953–1959.
[7] A.N. Simakov, D.C. Wilson, S.A. Yi, J.L. Kline, D.S. Clark, J.L. Milovich, J.D. Salmonson, Steven H. Batha, Phys. Plasmas 21 (2) (2014) 022701.
[8] J. Lindl, Phys. Plasmas 2 (11) (1995) 3933–4024.

[9] B. Spears, D. Hicks, C. Velsko, M. Stoyer, H. Robey, D. Munro, S. Haan, O. Landen, A. Nikroo, H. Huang, J. Phys.: Conf. Ser. 112 (2008) 022003.
[10] O.L. Landen, T.R. Boehly, D.K. Bradley, D.G. Braun, D.A. Callahan, P.M. Celliers, G.W. Collins, E.L. Dewald, L. Divol, S.H. Glenzer, et al., Phys. Plasmas 17 (2010) 056301.
[11] R.E. Olson, R.J. Leeper, A. Nobile, J.A. Oertel, G.A. Chandler, K. Cochrane, S.C. Dropinski, S. Evans, S.W. Haan, J.L. Kaae, et al., Phys. Plasmas 11 (2004) 2778.
[12] J. Massen, G.D. Tsakiris, K. Eidmann, I.B. Földes, Th. Löwer, R. Sigel, S. Witkowski, H. Nishimura, T. Endo, H. Shiraga, et al., Phys. Rev. E 50 (1994) 6.
[13] C.A. Back, J.D. Bauer, J.H. Hammer, B.F. Lasinski, R.E. Turner, P.W. Rambo, O.L. Landen, L.J. Suter, M.D. Rosen, W.W. Hsing, Phys. Plasmas 7 (5) (2000) 2126–2134.
[14] A.S. Moore, T.M. Guymer, J. Morton, B. Williams, J.L. Kline, N. Bazin, C. Bentley, S. Allan, K. Brent, A.J. Comley, J. Quant. Spectrosc. Radiat. Transfer 159 (2015) 19–28.
[15] S. Hatchett (Ed.), Ablation Gas Dynamics of Low-Z Materials Illuminated By Soft X-Rays, Lawrence Livermore National Laboratory, 1991, UCRL-JC–108348.
[16] S. Atzeni, J. Meyer-Ter-Vehn, The Physics of Inertial Fusion, Oxford, 2004.
[17] HYADES is a commercial product of Cascade Applied Sciences email: larsen@casinc.com.
[18] R.M. More, K.H. Warren, D.A. Young, G.B. Zimmerman, Phys. Fluids 31 (10) (1988) 3059–3078.
[19] L. Berzak Hopkins, L. Divol, C. Weber, S. Le Pape, N.B. Meezan, J.S. Ross, R. Tommasini, S. Khan, D.D. Ho, J. Biener, et al., Phys. Plasmas 25 (2018) 080706.
[20] Steven W. Haan, Lectures to the High Energy Density Physics Summer School, Santa Cruz, 2002.
[21] R.E. Olson, G.A. Rochau, O.L. Landen, R.J. Leeper, Phys. Plasmas 18 (2011) 032706.
[22] A.S. Moore, S. Prisbrey, K.L. Baker, P.M. Celliers, J. Fry, T.R. Dittrich, K.J. Wu, M.L. Kervin, M.E. Schoff, M. Farrell, et al., High Energy Density Phys. 20 (2016) 23–28.
[23] J.L. Kline, J.D. Hager, Matter Radiat. Extremes 2 (2017) 16.